An Autofocus Method for Backprojection Imagery in Synthetic Aperture Radar

Joshua N. Ash, Member, IEEE

Abstract—In this letter, we present an autofocus routine for backprojection imagery from spotlight-mode synthetic aperture radar data. The approach is based on maximizing image sharpness and supports the flexible collection and imaging geometries of BP, including wide-angle apertures and the ability to image directly onto a digital elevation map. While image-quality-based autofocus approaches can be computationally intensive, in the backprojection setting, we demonstrate a natural geometric interpretation that allows for optimal single-pulse phase corrections to be derived in closed form as the solution of a quartic polynomial. The approach is applicable to focusing standard backprojection imagery, as well as providing incremental focusing in sequential imaging applications based on autoregressive backprojection. An example demonstrates the efficacy of the approach applied to real data for a wide-aperture backprojection image.

Index Terms—Autofocus, autoregressive backprojection (ARBP), convolution BP (CBP) imaging, synthetic aperture radar (SAR).

I. INTRODUCTION

EASUREMENTS in synthetic aperture radar (SAR) are susceptible to unknown platform motion and varying atmospheric propagation delays. Both effects result in demodulation timing errors that may be modeled as unknown phase shifts on each pulse of the collected phase history data $\tilde{p}_{\theta}(r) = e^{j\phi}p_{\theta}(r)$, where ϕ is the phase error for the given pulse, $p_{\theta}(r)$ is the range-compressed pulse return from azimuth position θ , and $\tilde{p}_{\theta}(r)$ is the phase-corrupted measurement [1]. The phase errors induce blurring in subsequent SAR imagery, and it is the role of an autofocus algorithm to mitigate these effects. Traditional autofocus routines, such as phase gradient autofocus (PGA) [2], function as a postprocessing step operating on preformed SAR images and make the following assumptions.

1) A Fourier transform relationship exists between the image domain $z_{nm} \in \mathbb{C}$ and the range-compressed phase history domain $\tilde{G}_{nk} \in \mathbb{C}$

$$\tilde{G}_{nk} = \mathcal{F}_m(z_{nm}) \tag{1}$$

Manuscript received October 22, 2010; accepted March 14, 2011. Date of publication August 18, 2011; date of current version December 23, 2011. This work was supported by the U.S. Air Force Research Laboratory under Award FA8650-07-D-1220. Any opinions, findings, conclusions, or recommendations expressed in this letter are those of the author and do not necessarily reflect the views of the U.S. Air Force.

The author is with the Department of Electrical and Computer Engineering, The Ohio State University, Columbus, OH 43210 USA (e-mail: ashi@ece.osu.edu).

Color versions of one or more of the figures in this paper are available online at http://ieeexplore.ieee.org.

Digital Object Identifier 10.1109/LGRS.2011.2161456

- where z_{nm} denotes image domain data with n and m indexing range and cross-range, respectively, \tilde{G}_{nk} denotes the measured range-compressed sample for the nth range bin and kth azimuth position, and $\mathcal{F}_m(\cdot)$ denotes a 1-D discrete Fourier transform with uniform sampling along the cross-range (m) dimension.
- Phase errors are applied purely in the cross-range dimension

$$\tilde{p}_{\theta_k}(r_n) \equiv \tilde{G}_{nk} = G_{nk} e^{j\phi_k} \tag{2}$$

where θ_k is the azimuth position of the kth pulse, r_n denotes the range value of the nth range bin, G_{nk} denotes the uncorrupted range-compressed phase history, and ϕ_k is the phase error applied to pulse k.

These assumptions only hold for axis-aligned imagery collected over small aperture angles—where all pulses are approximately parallel. In this letter, we present a computationally efficient autofocus method compatible with the backprojection (BP) approach to SAR image formation, which directly supports a broader class of collection and imaging geometries, including wide-angle apertures, near- and far-field collections, arbitrary flight paths, and the ability to image directly onto a digital elevation map (DEM).

Our autofocus approach is based on maximizing image sharpness

$$s(\hat{\phi}) = \sum_{i} \Psi\left(v_i(\hat{\phi})\right) \tag{3}$$

where $v_i(\hat{\phi})$, is the intensity of the *i*th pixel of the image resulting from a particular set of phase error estimates $\hat{\phi}$, and $\Psi(x)$ is a convex function. In (3) and the remainder of this letter, it is more convenient to use a single index i for the pixels of an image z. There are many possible forms for $\Psi(x)$; however, the intensity-squared metric $\Psi(x) = x^2$ is known to apply equal emphasis on brightening bright points as it does on darkening shadows and has been empirically shown to work well on a variety of scene types [3]. Furthermore, this metric has been shown to produce phase error estimates equivalent to maximum likelihood estimates under particular conditions [4]. In this letter, we demonstrate that, for backprojection imagery, the optimal sharpness-maximizing phase may be determined on a per-pulse basis in closed form. The computational efficiency is achieved by identifying the phase optimization problem with a basic ellipsoidal geometry problem solvable by finding the minimum root of a quartic polynomial. This solution may be used within a coordinate descent framework to focus a standard backprojection image with respect to all pulses, or it may be

used to directly focus update frames in sequential imagery provided by autoregressive backprojection (ARBP) [5].

While autofocus for SAR under the two earlier stated assumptions has been considered extensively, to our knowledge, [6] is the only work considering autofocus under more general collections and with BP imaging. The method in [6] estimates phase corrections by employing PGA on an intermediate rangebearing grid, but the approach is only applicable for a restricted set of blurring kernels. Similar to this letter, joint imaging and focusing is considered in [7]—although based on ℓ_1 -regularized imaging, not backprojection.

II. AUTOFOCUS IN BACKPROJECTION IMAGING

A. Standard Convolution Backprojection

In the convolution backprojection (CBP) approach to SAR image formation, the image value for pixel i corresponding to ground-plane coordinates $q_i = [x_i \ y_i]$ is computed as [8]

$$z_{i} = \int_{\theta_{\min}}^{\theta_{\max}} \int_{\omega_{\min}}^{\omega_{\max}} p_{\theta}(\omega) e^{j\omega d(\mathbf{q}_{i})} |\omega| W_{r}(\omega) W_{x}(\theta) d\omega d\theta \qquad (4)$$

where $[\theta_{\min}, \theta_{\max}]$ and $[\omega_{\min}, \omega_{\max}]$ denote the azimuth and frequency support of the collection, respectively, $W_r(\omega)$ and $W_x(\theta)$ are apodization windows to control sidelobe levels in the range and cross-range dimensions, respectively, and $p_{\theta}(\omega)$ is the Fourier transform of the range profile at angle θ . The quantity $d(\mathbf{q}_i)$ denotes the position that point \mathbf{q}_i appears in the range profile. When the platform is in the far field, $d(\mathbf{q}_i) = x_i \cos \theta_k + y_i \sin \theta_k$ for pulse k. Other formulations of $d(\mathbf{q}_i)$ account for near-field imaging or imaging to a DEM [9]. As collected phase history data are discrete, in practice, (4) is written as a discrete sum over the number of pulses K

$$Q_k(r) = \mathcal{F}^{-1} \left\{ p_{\theta_k}(\omega) |\omega| W_r(\omega) \right\}$$
 (5)

$$z_i = \sum_{k=1}^{K} Q_k \left(d(\boldsymbol{q}_i) \right) W_x(\theta_k)$$
 (6)

where the inverse discrete Fourier transform in (5) yields the filtered range profile for pulse k, and the backprojection step is performed in (6).

Let the vector $\boldsymbol{b}_k = \{Q_k(d(\boldsymbol{q}_i))W_x(\theta_k)\}_i$ denote the filtered backprojection of pulse k over all pixels i of interest. In the absence of phase errors, the focused (vectorized) image is computed as

$$z = \sum_{k} b_{k}. \tag{7}$$

When the pulses are subject to phase errors, we see from (5) that the backprojections become phase corrupted as well $b_k \to \tilde{b}_k = b_k e^{j\phi_k}$, and $\sum \tilde{b}_k$ does not form a focused image. The objective of the autofocus algorithm is to produce phase estimates $\hat{\phi} = \{\hat{\phi}_1 \dots \hat{\phi}_K\}$ such that the image quality of

$$z = \sum_{k} \tilde{b}_{k} e^{-j\hat{\phi}_{k}} \tag{8}$$

is maximized over a given metric. As motivated earlier, we consider the sharpness metric $s(\hat{\phi}) = \sum_i v_i^2$, where $v_i = z_i z_i^*$ is the intensity of the *i*th pixel. Thus, the optimal correction is

$$\hat{\boldsymbol{\phi}} = \arg\max_{\boldsymbol{\phi}} s(\boldsymbol{\phi}). \tag{9}$$

As the optimization in (9) has no closed-form solution, we resort to an iterative method based on coordinate descent. A similar approach for polar-formatted images was considered in [10]. In the backprojection case, we will demonstrate that the optimal phase error correction for each pulse may be determined in closed form within the coordinate descent framework.

In coordinate descent optimization, each parameter is optimized, in turn, while holding all other parameters fixed. Because the parameters are interdependent, optimization over the entire set of parameters must be performed a number of times—called iterations. Let $\hat{\phi}_k^i$ denote the kth coordinate (kth pulse phase correction) of the ith iteration; then, the coordinate descent estimate at the next iteration i+1 is defined as

$$\hat{\phi}_{k}^{i+1} = \arg\max_{\phi} s\left(\hat{\phi}_{1}^{i+1}, \dots, \hat{\phi}_{k-1}^{i+1}, \phi, \hat{\phi}_{k+1}^{i}, \dots, \hat{\phi}_{K}^{i}\right),$$

$$k = 1, \dots, K. \tag{10}$$

Consider the reflectivity image $z(\phi)$ at the ith iteration parameterized by the unknown phase of pulse k while holding all other phases constant

$$z(\phi) = \sum_{p=1}^{k-1} e^{-j\hat{\phi}_p^{i+1}} \tilde{\boldsymbol{b}}_p + \sum_{p=k+1}^K e^{-j\hat{\phi}_p^{i}} \tilde{\boldsymbol{b}}_p + e^{-j\phi} \tilde{\boldsymbol{b}}_k \quad (11)$$
$$= \boldsymbol{x} + e^{-j\phi} \boldsymbol{y} \tag{12}$$

where x comprises the backprojection sum of all pulses (with current corrections) other than pulse k and y is the uncorrected backprojection of pulse k. The associated intensity of the ith pixel of $z(\phi)$ is

$$v_{i} = z_{i}z_{i}^{*} = (x_{i} + e^{-j\phi}y_{i}) \left(x_{i}^{*} + e^{j\phi}y_{i}^{*}\right)$$

$$= \underbrace{|x_{i}|^{2} + |y_{i}|^{2}}_{(\mathbf{v}_{0})_{i}} + \underbrace{2\Re\left(y_{i}^{*}x_{i}e^{j\phi}\right)}_{(\mathbf{v}_{\phi})_{i}}.$$
(13)

In vector form, the "intensity image" may be written as $v = v_0 + v_{\phi}$, where v_0 is constant and v_{ϕ} depends on the unknown phase of pulse k. The sharpness metric over all pixels may be written as

$$\sum_{i} v_i^2 = \|\mathbf{v}\|^2 \tag{15}$$

and interpreted as the squared length of v. Hence, the optimal phase correction for pulse k at iteration i is the value of ϕ that maximizes the length of v.

We observe that the set of backprojections $\{\tilde{b}_k\}$ for all pulses $\{k\}$ only needs to be computed once, irrespective of the number of coordinate descent iterations. However, \tilde{b}_k is only needed when optimizing for ϕ_k . Thus, in memory-limited cases, \tilde{b}_k can be computed as needed without storing the backprojections of all pulses.

B. Autoregressive Backprojection

ARBP is a recently proposed image formation method applicable to persistent sensing applications where an airborne platform continuously circles a scene of interest and a sequence of SAR images is to be produced, as in, e.g., a SAR video [5]. While standard CBP (7) sums the backprojections from a large number of previous *pulses*, in sequential imaging, ARBP exploits previously generated *images* in order to reduce the memory and computational requirements of generating the current image

$$I_k = \sum_{m=1}^{M} \alpha_m I_{k-m} + \beta b_k \tag{16}$$

where M is the autoregression order (typically $M \leq 3$), I_k is the vectorized image at aperture position k, b_k is the current pulse filtered and backprojected over the pixels of interest, and $\{\alpha_k\}$ and β are constants controlling the coherent azimuth integration angle and the cross-range sidelobe structure. When the current pulse contains a phase error and the previous images I_{k-1}, I_{k-2}, \ldots have been focused, the current image may be parameterized by a phase correction ϕ of the current pulse $I_k = \sum_{m=1}^M \alpha_m I_{k-m} + e^{-j\phi} \beta b_k$ and optimized for maximal sharpness. Letting $\mathbf{x} = \sum_{m=1}^M \alpha_m I_{k-m}$ and $\mathbf{y} = \beta b_k$, the current image may be written as $\mathbf{z} = \mathbf{x} + e^{-j\phi} \mathbf{y}$. Thus, given that previous images have been focused, focusing the current image in an ARBP update is mathematically equivalent to maximizing the sharpness over a single coordinate in the coordinate descent approach to sharpness maximization in standard BP.

III. GEOMETRIC INTERPRETATION

The previous section demonstrated that candidate per-pulse-corrected BP images and ARBP images may be written as $\boldsymbol{z} = \boldsymbol{x} + e^{-j\phi}\boldsymbol{y}$ and that elements of the intensity image may be written as $v_i = (v_0)_i + (v_\phi)_i$, where $(v_\phi)_i = 2\Re(y_i^*x_ie^{j\phi})$. By defining the vectors \boldsymbol{a} and \boldsymbol{b} with elements $a_i = 2\Re(y_i^*x_i)$ and $b_i = -2\Im(y_i^*x_i)$, \boldsymbol{v}_ϕ may be written as

$$\boldsymbol{v}_{\phi} = \boldsymbol{a}\cos\phi + \boldsymbol{b}\sin\phi \tag{17}$$

which has the interpretation of an ellipse, even though a and b are not necessarily orthogonal. Hence, for an $N \times N$ image, $v = v_0 + v_\phi$ traces out an ellipse on a 2-D plane embedded in \mathbb{R}^{N^2} . The plane is spanned by $a, b \in \mathbb{R}^{N^2}$ and offset from the origin by $v_0 \in \mathbb{R}^{N^2}$. As shown in Fig. 1, the phase ϕ indexes the ellipse, and the optimal phase $\hat{\phi}$ maximizes the length of v.

The displacement vector v_0 may be decomposed into a portion in the a,b plane and a portion perpendicular to this plane. The perpendicular component contributes a fixed ϕ -independent amount to the length $\|v\|$ and may be ignored for optimization purposes. As such, we may work completely in the 2-D plane $\mathcal S$ spanned by a,b and define a new 2-D $\mathcal S$ -coordinate system with the ellipse at the origin (see Fig. 1). We are free to choose any basis $\{e_1,e_2\}$ for $\mathcal S$, but we use an orthonormalization of a,b for convenience

$$e_1 = \frac{a}{\|a\|}$$
 $e_2 = \frac{b - e_1 e_1^T b}{\|b - e_1 e_1^T b\|}.$ (18)

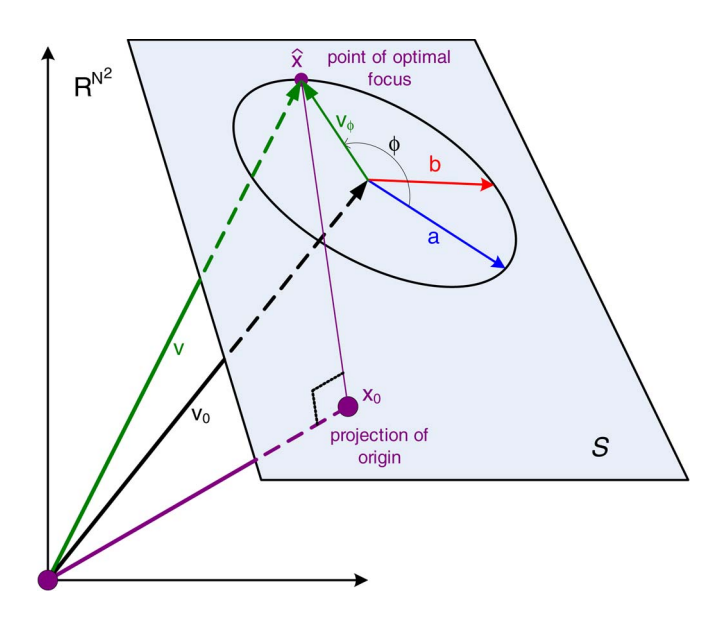


Fig. 1. Geometry of the autofocus problem. Candidate phase corrections map out a displaced ellipse, and the optimal correction maximizes the length of v.

In the new coordinate system, a and b become

$$\tilde{a} \equiv \begin{bmatrix} \tilde{a}_1 \\ \tilde{a}_2 \end{bmatrix} = \boldsymbol{E}^T \boldsymbol{a} \qquad \tilde{\boldsymbol{b}} \equiv \begin{bmatrix} \tilde{b}_1 \\ \tilde{b}_2 \end{bmatrix} = \boldsymbol{E}^T \boldsymbol{b}$$
 (19)

where $E = [e_1 \ e_2]$. Finally, the origin of \mathbb{R}^{N^2} must be projected onto \mathcal{S} . Relative to the origin of \mathcal{S} , the origin of \mathbb{R}^{N^2} is at $-v_0$. After projecting and reparameterizing, this point becomes

$$x_0 = E^T (EE^T)(-v_0) = -E^T v_0.$$
 (20)

Hence, the final optimization problem reduces to a basic geometry problem in \mathbb{R}^2 where one has to find the point \hat{x} , on an origin-centered ellipse, that lies farthest from the given point x_0 .

IV. PHASE OPTIMIZATION

Having reduced the phase estimation problem to one of basic geometry, we now present a closed-form solution for the optimal phase correction. The approach is similar to the work in [11], extended for maximal distance and to support rotated ellipses defined by oblique axes. At the farthest point \hat{x} , the vector $x_0 - \hat{x}$ will be parallel to the normal n(x) of the ellipse

$$\boldsymbol{x}_0 - \hat{\boldsymbol{x}} = \alpha \, \boldsymbol{n}(\hat{\boldsymbol{x}}) \tag{21}$$

for some real constant α . The ellipse in \mathcal{S} may be written parametrically $\boldsymbol{x}(\phi) = [x_1 \ x_2]^T = \tilde{\boldsymbol{a}} \cos \phi + \tilde{\boldsymbol{b}} \sin \phi$ or implicitly

$$f(x) \equiv x^T R x = 1 \tag{22}$$

with

$$\boldsymbol{R} = \begin{bmatrix} r_1 & r_3 \\ r_3 & r_2 \end{bmatrix}. \tag{23}$$

The elements of ${m R}$ equating the implicit ellipse to the parametric form can be shown to be

$$r_1 = \left(\tilde{a}_2^2 + \tilde{b}_2^2\right)/c \tag{24}$$

$$r_2 = \left(\tilde{a}_1^2 + \tilde{b}_1^2\right)/c \tag{25}$$

$$r_3 = -(\tilde{a}_1 \tilde{a}_2 + \tilde{b}_1 \tilde{b}_2)/c \tag{26}$$

where $c=(\tilde{a}_2\tilde{b}_1-\tilde{a}_1\tilde{b}_2)^2$. Using the implicit form, the normal is computed from the gradient of $f(\boldsymbol{x}),\ \boldsymbol{n}(\boldsymbol{x})\equiv\nabla f(\boldsymbol{x})=2\boldsymbol{R}\boldsymbol{x}$. Thus, absorbing the factor of two into the unknown α , $\boldsymbol{x}_0-\hat{\boldsymbol{x}}=\alpha\boldsymbol{R}\hat{\boldsymbol{x}}$ and

$$\hat{\boldsymbol{x}} = (\alpha \boldsymbol{R} + \boldsymbol{I})^{-1} \boldsymbol{x}_0. \tag{27}$$

Let $oldsymbol{R} = oldsymbol{V} oldsymbol{\Lambda} oldsymbol{V}^T$ denote the eigendecomposition of $oldsymbol{R}$; then, we have

$$(\alpha \mathbf{R} + \mathbf{I}) = \mathbf{V}(\alpha \mathbf{\Lambda} + \mathbf{I})\mathbf{V}^{T}$$
(28)

for the eigendecomposition of $(\alpha R + I)$. Substituting (27) and (28) into (22), we obtain

$$1 = \boldsymbol{x}_0 (\alpha \boldsymbol{R} + \boldsymbol{I})^{-1} \boldsymbol{R} (\alpha \boldsymbol{R} + \boldsymbol{I})^{-1} \boldsymbol{x}_0$$
 (29)

$$= \boldsymbol{x}_0^T \boldsymbol{V} (\alpha \boldsymbol{\Lambda} + \boldsymbol{I})^{-1} \boldsymbol{V}^T (\boldsymbol{V} \boldsymbol{\Lambda} \boldsymbol{V}^T) \boldsymbol{V} (\alpha \boldsymbol{\Lambda} + \boldsymbol{I})^{-1} \boldsymbol{V}^T \boldsymbol{x}_0$$
(30)

$$= \boldsymbol{x}_0^T \boldsymbol{V} (\alpha \boldsymbol{\Lambda} + \boldsymbol{I})^{-1} \boldsymbol{\Lambda} (\alpha \boldsymbol{\Lambda} + \boldsymbol{I})^{-1} \boldsymbol{V}^T \boldsymbol{x}_0$$
 (31)

$$= \boldsymbol{x}_0^T \boldsymbol{V} \begin{bmatrix} \frac{\lambda_1}{(\alpha \lambda_1 + 1)^2} & 0\\ 0 & \frac{\lambda_2}{(\alpha \lambda_2 + 1)^2} \end{bmatrix} \boldsymbol{V}^T \boldsymbol{x}_0$$
 (32)

where λ_1 and λ_2 are the eigenvalues of \mathbf{R} , and $\mathbf{\Lambda} = \operatorname{diag}(\{\lambda_1, \lambda_2\})$.

Letting $[\beta_1, \beta_2]^T = V^T x_0$, (32) may be written as

$$q(\alpha) = \beta_1^2 \frac{\lambda_1}{(\alpha \lambda_1 + 1)^2} + \beta_2^2 \frac{\lambda_2}{(\alpha \lambda_2 + 1)^2} - 1 = 0$$
 (33)

which has the same roots as the fourth-order polynomial

$$p(\alpha) \equiv \sum_{i=0}^{4} \gamma_i \alpha^i = 0 \tag{34}$$

where

$$\gamma_0 = \lambda_1 \beta_1^2 + \lambda_2 \beta_2^2 - 1 \tag{35}$$

$$\gamma_1 = 2\lambda_1 \left(\lambda_2 \beta_2^2 - 1 \right) + 2\lambda_2 \left(\lambda_1 \beta_1^2 - 1 \right) \tag{36}$$

$$\gamma_2 = (\lambda_1 \beta_1^2 - 1) \lambda_2^2 + (\lambda_2 \beta_2^2 - 1) \lambda_1^2 - 4\lambda_1 \lambda_2$$
 (37)

$$\gamma_3 = -2\lambda_1 \lambda_2 (\lambda_1 + \lambda_2) \tag{38}$$

$$\gamma_4 = -(\lambda_1 \lambda_2)^2. \tag{39}$$

The roots of $p(\alpha)$ may be found from the eigenvalues of the polynomial's 4×4 companion matrix [12] or any other computationally efficient rooting algorithm. In general, $p(\alpha)$ will have up to four real roots, and it is straightforward to show that the closest and farthest points on the ellipse correspond to the largest and smallest purely real roots, respectively [11]. Letting

 $\hat{\alpha}$ denote the smallest real root, the optimal phase correction $\hat{\phi}$ may be computed as

$$\hat{\phi} = \tan^{-1} \left(\frac{\sin \hat{\phi}}{\cos \hat{\phi}} \right) \tag{40}$$

where

$$\begin{bmatrix} \cos \hat{\phi} \\ \sin \hat{\phi} \end{bmatrix} = [\tilde{a} \ \tilde{b}]^{-1} (\hat{\alpha} R + I)^{-1} x_0 \tag{41}$$

and a four-quadrant inverse tangent is used in (40).

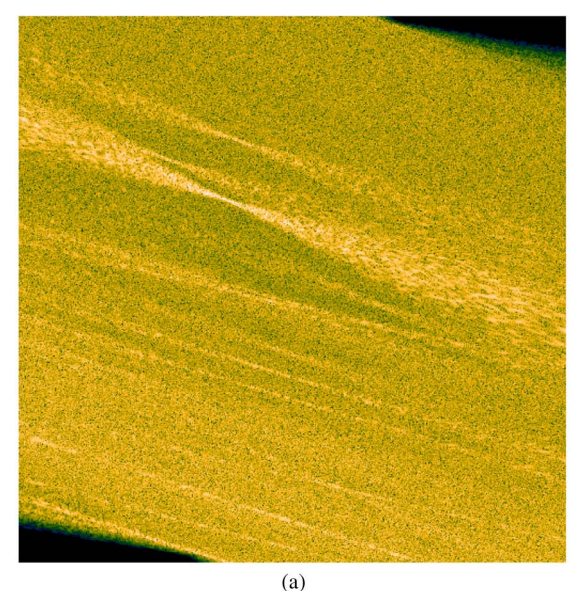
V. EXAMPLE

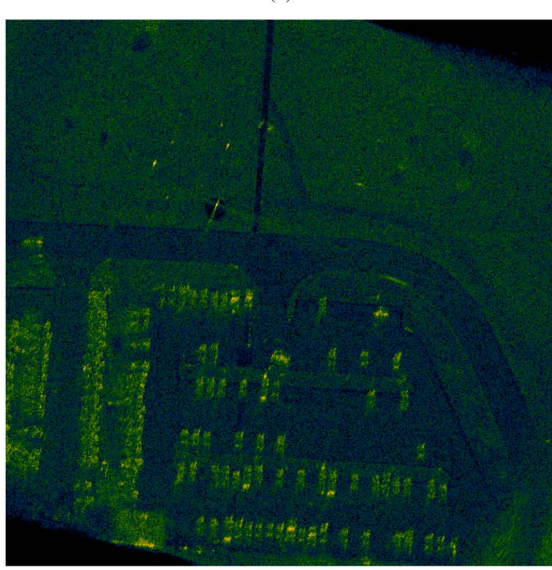
In this section, we demonstrate results on real data from the Gotcha Public Release Dataset [13]—an X-band collection with 9.6-Hz center frequency and 640-MHz bandwidth. We note that, for this bandwidth, a 3° aperture provides approximately equal range and cross-range support in the transduced phase history data. The data were collected in circular spotlight mode with an approximate standoff of 10 km. The released data have an azimuth sample rate of approximately 117 pulses per degree and have a phase history that is already focused. We therefore artificially introduce phase errors into the pulse history for this example. In contrast to the traditional autofocus literature, we induce phase errors directly on the pulses making up the annular aperture—not on range-compressed data obtained by a 1-D inverse fast Fourier transform applied to a preformed image. The phase error applied across the annular aperture was white Gaussian noise with zero mean and a standard deviation of π radians. Fig. 2 shows the resulting CBP images obtained for a 25° aperture without and with the autofocus method applied. The focused image resulted from four iterations of coordinate descent using an initial phase estimate of zero for all pulses. Fig. 2(c) shows the resulting sharpness after each iteration, relative to the initial unfocused image in Fig. 2(a).

VI. CONCLUSION

In this letter, we have considered an autofocus method for backprojection imagery from spotlight-mode SAR data and demonstrated that the optimal per-pulse phase correction under the image sharpness metric has an appealing ellipsoidal geometric interpretation in a reduced subspace. Exploiting this geometry enabled us to solve for the optimal per-pulse phase correction in closed form. This method may be used in a coordinate descent framework for efficient focusing over multiple pulses in a CBP image, or it may be integrated in an ARBP framework for *in situ* focusing of sequentially updated images.

Finally, we note that, as the method herein was developed under more general conditions than the assumptions described in Section I, it naturally supports the more restrictive scenario described there, even for imagery produced via the polar format algorithm (PFA). A phase-corrected PFA image may be written as $z_{nm} = \sum_k \tilde{G}_{nk} e^{j(2\pi/N)km} e^{-j\hat{\phi}_k}$, where \tilde{G}_{nk} represents





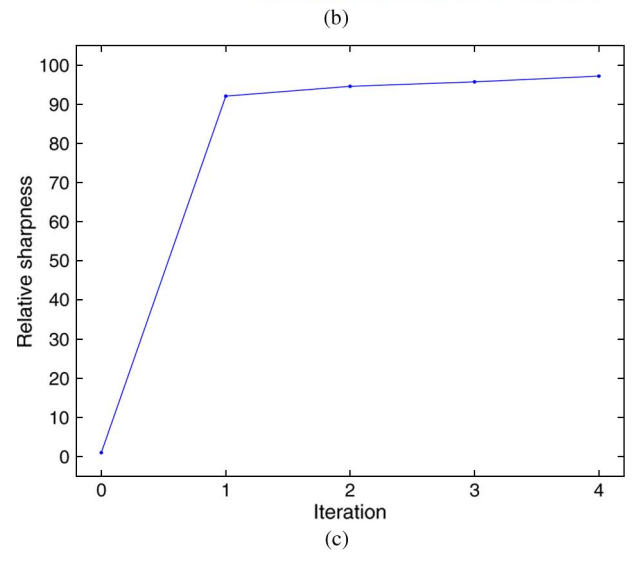


Fig. 2. Example backprojection SAR imagery of a parking lot using a wide 25° aperture, (a) without and (b) with autofocus. (c) Relative sharpness versus iteration count for the algorithm.

measured data after polar formatting and range compression. In matrix form, the image $Z = \{z_{nm}\}$ may be written as

$$Z = \sum_{k} B_k e^{-j\hat{\phi}_k} \tag{42}$$

where the elements of the matrix B_k are equal to $(B_k)_{nm} = \tilde{G}_{nk}e^{j(2\pi/N)km}$. As the form of (42) is identical to that of (8), the geometric interpretation and phase optimization method developed for backprojection may be directly applied in a polar format setting as well.

REFERENCES

- C. V. Jakowatz, D. E. Wahl, P. H. Eichel, D. C. Ghiglia, and P. A. Thompson, Spotlight-Mode Synthetic Aperture Radar: A Signal Processing Approach. Berlin, Germany: Springer-Verlag, 1996.
- [2] D. E. Wahl, P. H. Eichel, D. C. Ghiglia, and C. V. Jakowatz, "Phase gradient autofocus—A robust tool for high resolution SAR phase correction," *IEEE Trans. Aerosp. Electron. Syst.*, vol. 30, no. 7, pp. 827–835, Jul. 1994.
- [3] J. R. Fienup and J. J. Miller, "Aberration correction by maximizing generalized sharpness metrics," *J. Opt. Soc. Amer. A, Opt. Image Sci.*, vol. 20, no. 4, pp. 609–620, Apr. 2003.
- [4] T. J. Schulz, "Optimal sharpness function for SAR autofocus," *IEEE Signal Process. Lett.*, vol. 14, no. 1, pp. 27–30, Jan. 2007.
- [5] R. L. Moses and J. N. Ash, "Recursive SAR imaging," in *Proc. SPIE—Algorithms Synthetic Aperture Radar Imagery*, Mar. 2008, vol. 6970, pp. 69700P-1–69700P-12.
- [6] C. V. Jakowatz and D. E. Wahl, "Considerations for autofocus of spotlight-mode SAR imagery created using a beamforming algorithm," in *Proc. SPIE—Algorithms Synthetic Aperture Radar Imagery XVI*, 2009, vol. 7337, pp. 73370A-1–73370A-9.
- [7] N. O. Önhon and M. Çetin, "A nonquadratic regularization-based technique for joint SAR imaging and model error correction," in *Proc. SPIE—Algorithms Synthetic Aperture Radar Imagery XVI*, 2009, vol. 7337, p. 73370C.
- [8] M. Desai and W. Jenkins, "Convolution backprojection image reconstruction for spotlight mode synthetic aperture radar," *IEEE Trans. Image Process.*, vol. 1, no. 4, pp. 505–517, Oct. 1992.
- [9] C. Jakowatz, D. Wahl, and D. Yocky, "Beamforming as a foundation for spotlight-mode SAR image formation by backprojection," in *Proc. SPIE—Algorithms Synthetic Aperture Radar Imagery*, Mar. 2008, vol. 6970, p. 69700Q.
- [10] T. J. Kragh, "Monotonic iterative algorithm for minimum-entropy autofocus," in *Proc. Adapt. Sensor Array Process. Workshop*, Lexington, MA, Jun. 2006.
- [11] J. C. Hart, "Distance to an ellipsoid," in *Graphics Gems IV*. San Mateo, CA: Morgan Kaufmann, 1994.
- [12] G. Golub and C. Van Loan, *Matrix Computations*, 3rd ed. Baltimore, MD: The Johns Hopkins Univ. Press, 1996.
- [13] C. Casteel, L. Gorham, M. Minardi, S. Scarborough, K. Naidu, and U. Majumder, "A challenge problem for 2-D /3-D imaging of targets from a volumetric data set in an urban environment," in *Proc.* SPIE—Algorithms Synthetic Aperture Radar Imagery XIV, E. G. Zelnio and F. D. Garber, Eds., 2007, vol. 6568, p. 65680D.